Enhanced Electrochemical Performance of $LiNi_{0.8}Co_{0.1}Mn_{0.1}O_2$ with SiO_2 Surface Coating Via Homogeneous Precipitation

Lintao Dou,[a] Pu Hu,*[a] Chaoqun Shang,[a] Heng Wang,[a] Dongdong Xiao,*[b] Utkarsh Ahuja,[c] Katerina Aifantis,[c] Zhanhui Zhang,*[a] and Zhiliang Huang[a]

Ni-rich $LiNi_{0.8}Co_{0.1}Mn_{0.1}O_2$ (NCM811) has been considered as a promising cathode material for high energy density lithium-ion batteries. However, it experiences undesirable interfacial side-reactions with the electrolyte, which lead to a rapid capacity decay. In this work, a homogeneous precipitation method is proposed for forming a uniform silicon dioxide (SiO_2) coating on the NCM811 surface. The strong Si–O network provided a stable protective layer between the NCM811 active material and electrolyte to improve the electrochemical stability. As a result, the NCM811@SiO_2 cathode showed superior cycling stability (84.9% after 100 cycles at 0.2 C) and rate capability (142.7 mA h g^{-1} at 5 C) compared to the pristine NCM811 cathode (56.6% after 100 cycles, 127.9 mA h g^{-1} at 5 C). Moreover, the SiO_2 coating effectively suppressed voltage decay and pulverization of the NCM811 particles during long term cycling. This uniform coating technique offers a viable approach for stabilizing Ni-rich cathode materials for high-energy density lithium-ion batteries.

1. Introduction

It is well known that lithium-ion batteries (LIBs) are the most widely used energy storage devices in portable electronic devices and in electric vehicles.[1] Among various cathodes, Ni-rich $LiNi_{0.8}Co_{0.1}Mn_{0.1}O_2$ (NCM811) materials have attracted a lot of attention as promising candidates, for higher energy density LIBs, primarily due to their high voltage and specific capacity (~200 mA h g^{-1}).[2] In terms of Ni content, the Ni-rich cathodes (NCM811) have advantages in gravimetric capacity, compared with the state-of-the-art $LiNi_{06}Co_{0.2}Mn_{0.2}O_2$ (NCM622). However, significant capacity decay occurs upon cycling due to the mixing of Li^+/Ni^{2+} cations in the crystal structure, dissolution of the transition metals and undesired interfacial side reaction between the NCM811 active material and electrolyte.[3] During long-term cycling, the active materials particles undergo cracking, which leads to a loss of active material and an increase in surface area, thereby exacerbating structural and surface instabilities, and ultimately reducing the capacity.[4] In addition, Ni-rich cathode materials are highly sensitive to H_2O and CO_2, which leads to the formation of LiOH and Li_2CO_3 impurities on the surface of the NCM811 particles. Such alkaline impurities cause gelation of the slurry during electrode preparation and deterioration of the battery life.[5]

A most promising technique for suppressing the undesired side reactions that take place between the NCM811 particles and the electrolyte,[6] but also suppress the irreversible phase transformations[7] that can occur during cycling is to coat the cathode active particle surface with a uniform thin protective layer that is inert to the electrolyte. Oxides, such as SiO_2,[7,8] ZrO_2,[9] TiO_2,[10] Al_2O_3,[11] et al. are commonly employed as such coating materials, among which SiO_2 is of the promising since it is inexpensive, precursors are abundantly available and is environmentally benign. Specifically, amorphous SiO_2 has been utilized as a coating on a variety of cathode materials, such as $LiMn_2O_4$,[12] $LiFePO_4$,[13] $LiNi_{0.5}Mn_{1.5}O_4$,[14] and $LiNi_{0.6}Co_{0.2}Mn_{0.2}O_2$,[15] resulting in improved performance. It was recently reported that the cyclability and rate capability of NCM811 was improved by coating SiO_2 and they attributed this improved performance to the suppress the irreversible phase transformation and play a role in obstacle to protect the NCM811 from electrolyte due to the coating.[7] Other materials such as $FePO_4$ (LFP3)[16] and polymers[17] (PVP and PANI) have also been used successfully to improve the performance of NCM811. Specifically, for LFP3@NCM811 the initial discharge capacity was 218.8 mA h g^{-1} at 0.1 C, and 151.4 mA h g^{-1} at 5 C, which is 15 mA h g^{-1} higher than that of the uncoated NCM811 cathode. For NCM811@PANI-PVP 88.7% retention was observed after 100 cycles at 200 mA g^{-1}) and 152 mA h g^{-1} at 1000 mA g^{-1}.

It is therefore seen that producing a uniform and continuous surface coating is critical to develop high performance Ni-rich cathode materials. Such an artificial physical barrier/surface

[a] L. Dou, Prof. P. Hu, Prof. C. Shang, Prof. H. Wang, Prof. Z. Zhang, Prof. Z. Huang
Hubei Key Laboratory of Plasma Chemistry and Advanced Materials, School of Materials Science and Engineering
Wuhan Institute of Technology
Wuhan, 430205, China
E-mail: hupu@wit.edu.cn
zzhlzu@163.com
[b] Prof. D. Xiao
Institute of Physics
Chinese Academy of Sciences
Beijing 100190, P. R. China
E-mail: dongdongxiao@iphy.ac.cn
[c] Dr. U. Ahuja, Prof. K. Aifantis
Department of Mechanical and Aerospace Engineering
University of Florida
Gainesville, Florida 32603, United States

Supporting information for this article is available on the WWW under https://doi.org/10.1002/celc.202101230

modification layer should be thin and homogenous, mechanically robust and electrochemically stable during operation and storage.[18] Traditional solid-state and heterogeneous deposition methods present inherent complications in controlling the thickness and uniformity of the surface layer.[19] The Stöber reaction is the most common method to fabricate silica particles with highly tailorable sizes and surface properties. The formation of silica based on this reaction involves two steps that are hydrolysis of tetraethyl orthosilicate (TEOS) and condensation of the intermediate of silanol groups (–Si–OH).[20] It is known that the reaction rate of the condensation step is much faster than hydrolysis and is greatly influenced by the temperature and pH of the solution.[21] Because hydrolysis of urea is sufficiently slow and occurs under acceptable temperatures, it is expected to be used as a precipitator to adjust the pH and the condensation rate for the homogeneous precipitations in the Stöber reaction.

In this study, a facile precipitation method is utilized to fabricate NCM811 particles coated with a homogeneous SiO_2 layer (NCM811@SiO_2). Urea-assisted condensation reaction was employed to ensure that the SiO_2 coating was uniform and continuous; this method has not been employed before for producing a SiO_2 coating on NCM811. The effects of the SiO_2 layer on the electrochemical performance of the NCM811 cathode was investigated by comparing with uncoated NCM811. Benefiting from the chemically inert coating, NCM811@SiO_2 shows superior cycling stability and rate capability compared to the pristine NCM811 cathode.

2. Results and Discussion

SiO_2 is uniformly coated on the surface of NCM811 via a urea-assisted homogeneous precipitation method, in which TEOS is used as Si source. As shown in Figure 1, the formation of a Si–O network covering includes the two steps of hydrolysis and condensation. TEOS is easily hydrolyzed into monomers and oligomers under acidic conditions, which disperses homogeneously in the solution and adsorbs on the surface of the NCM811 particles. The monomers and oligomers have a high chemical activity under acidic conditions, which can form a connection point with the surface of the cathode.[22] The addition of urea and its subsequent hydrolysis release ammonia. Urea is added to adjust the pH of the solution to alkaline. Under alkaline conditions, these monomers and oligomers easily undergo dehydration condensation to form a continuous O–Si–O network, which is uniformly attached to the surface of the NCM811 particles. After calcination, amorphous SiO_2 is formed. As shown in Figure S1, XRD patterns of pristine NCM811 and NCM811@SiO_2 materials show no obvious differences. All diffraction peaks coincide with hexagonal structured layered oxides with the $R\bar{3}m$ space group.[23] Therefore, deposition of SiO_2 does not change the layered structure of NCM811. The peak splitting of (006)/(102) and (108)/(110) can be clearly observed, demonstrating the highly ordered layered structure of the material.[24] The degree of splitting of the diffraction peaks of (006)/(102) and (108)/(110) reflects the integrity of the layered structure of the material and has a greater impact on the electrochemical performance of the material. The greater the splitting degree of the two pairs of diffraction peaks, the more complete the α-NaFeO2 type layered structure will be, and a better the electrochemical performance will be obtained. A diffraction peak for SiO_2 was not observed for NCM811@SiO_2, implying that the SiO_2 obtained after calcination might be amorphous. It is expected that such a continuous and uniform coating on the surface will act as a perfect superficial modification to improve the electrochemical performance of Ni-rich cathode materials.

The morphology of the as-obtained material is characterized by scanning electron microscopy (SEM). The pristine NCM811 particles have a double microstructure as they are secondary particles with a diameter of ~10 μm, comprised of primary particles that are 0.5–1 μm (Figure S2). The morphology and particle size of the NCM811 are well preserved after coating with SiO_2, suggesting that the homogeneous precipitation process has a negligible effect on the morphology of NCM811. However, high magnification SEM images of the uncoated NCM811 show a smooth surface with well-defined edges (Figure 2a, b). After coating, however, a rough surface with tiny specks is observed on its surface (Figure 2c, d). EDS shows a clear signal of Si (Figure S3) and EDS mappings of the NCM811@SiO_2 materials are provided in Figure 2e. Clearly, Ni, Co, Mn and Si are homogeneously distributed over the entire secondary particles. These observations demonstrate that the SiO_2 is uniformly coated on the surface of the NCM811 particles. In addition, high-resolution transmission electron microscopy (HRTEM) was performed to visualize the particle interior and its surface structure. Particularly, atomic-resolution high-angle annular dark field scanning transmission electron microscopy (HAADF-STEM) was employed. Figure 2f depicts the interior of a pristine NCM811 particles showing the well-defined crystal structure with a lattice spacing of 4.45 Å, which corresponds to the (003) plane of the ordered layered phase. The fast Fourier transform (FFT) pattern of Figure 2h presents well-defined spots on the (003), (104) and (101) planes that are coherent with the $R\bar{3}m$ space group. Since the intensity of the HAADF-STEM image is proportional to $Z^{\sim 1.7}$ (Z is atomic number), only heavy transition metal elements (Ni, Co, Mn) in the NCM811 can be

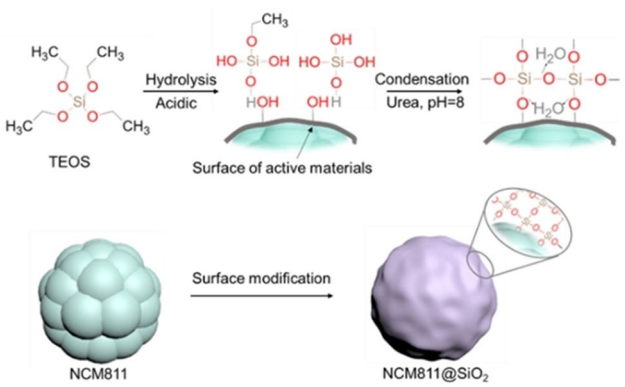

Figure 1. Schematic diagram of formation process of SiO_2 coating NCM811.

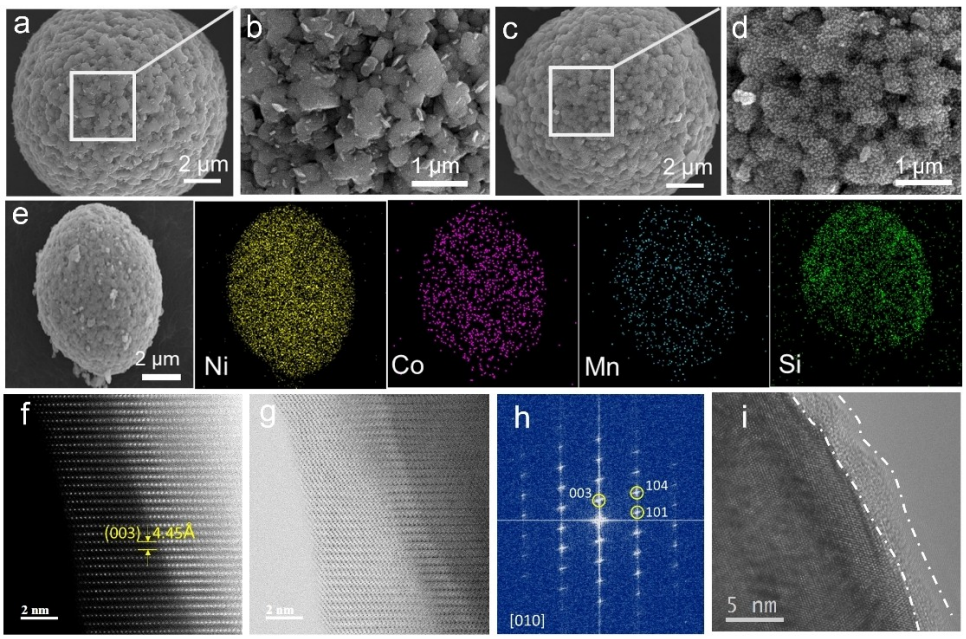

Figure 2. The SEM images of pristine NCM811 (a, b) and NCM811@SiO_2 (c, d); EDS elemental mapping of NCM811@SiO_2 (e); HAADF-STEM image (f) and HRTEM images (g) of pristine NCM811; The corresponding FFT of pristine NCM811 (h); HRTEM images of NCM811@SiO_2 (i).

visualized, hence the bright spots found in Li slabs in the Figure 2f imply the existence of Li^+/Ni^{2+} cations mixing, which is consistent with the XRD results. Figure 2g depicts the surface of the uncoated particle. Figure 2i is taken from a coated particle and it is clearly seen that the thin amorphous coating is ~3 nm.

The surface composition of the as-prepared materials is further investigated by XPS and FT-IR, shown in Figure 3. The XPS survey spectra confirms the existence of Si (Figure S4). The high-resolution XPS spectra as shown in Figure 3a, exhibits a peak at 101.90 eV corresponding to the Si 2p signal from the NCM811@SiO_2 that can be attributed to Si^{4+} from SiO_2.[14] The C 1s spectrum consists of three peaks at 284.8, 286.1 and 289.8 eV, which can be assigned to the carbon from C–C, C=O and Li_2CO_3 (Figure 3b). The pristine NCM811 displays higher intensity for the C 1s spectrum of Li_2CO_3, since the pristine NCM811 is commonly contained the Li_2CO_3 contaminant that originates from reactions of surface Li^+ with ambient CO_2 and H_2O. The O 1s at binding energies of 530.97 eV and 532.00 eV corresponds to lattice oxygen and surface oxygen, resulting from the surface CO_3^{2-}. An additional peak at 533.3 eV can be found for the NCM811@SiO_2 in Figure 3c, which can be attributed to the O spectrum of SiO_2. The FT-IR spectra of the pristine NCM811 and NCM811@SiO_2 samples are shown in Figure 3d. Characteristic peaks of the Si–O stretching vibration at 882 and 1064 cm^{-1} further confirm the formation of SiO_2.

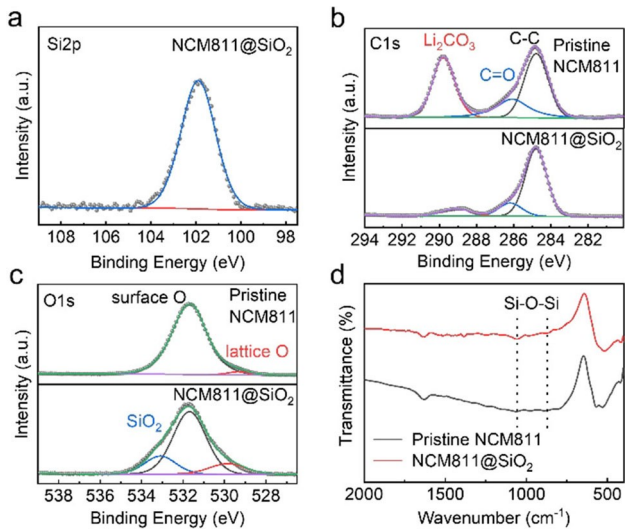

Figure 3. XPS spectra of C 1s (a), O 1s (b), Si 2p (c) and FT-IR spectra for the pristine NCM811 and NCM811@SiO_2 (d).

As mentioned the electrochemical performances of pristine NCM811 and NCM811@SiO_2 was tests evaluated at room temperature in coin cells at the potential range of 2.8 ~ 4.3 V. Figure 4a, compares the cycling stability of pristine NCM811 and NCM811@SiO_2 at 0.2 C. The initial discharge specific capacity of NCM811@SiO_2 is 208.4 mA h g^{-1}, slightly higher than that of the pristine NCM811 (204.3 mA h g^{-1}). After 100 cycles, the capacity for NCM811@SiO_2 is 172.8 mA h g^{-1}, indicating a retention of 84.9%. The pristine NCM811, had a much lower capacity of 114.3 mA h g^{-1}, corresponding to a retention of 56.6%. Furthermore, it can be seen that the NCM811@SiO_2 electrode delivers a higher coulombic efficiency (C.E.) and more stable values upon cycling (Figure 4a). These results demonstrate that the SiO_2 coating considerably improves the cycling stability of the NCM811 cathode. Cyclic voltammetry (CV) characterization is performed to investigate the Li^+ interaction/de-intercalation processes in pristine and coated NCM811

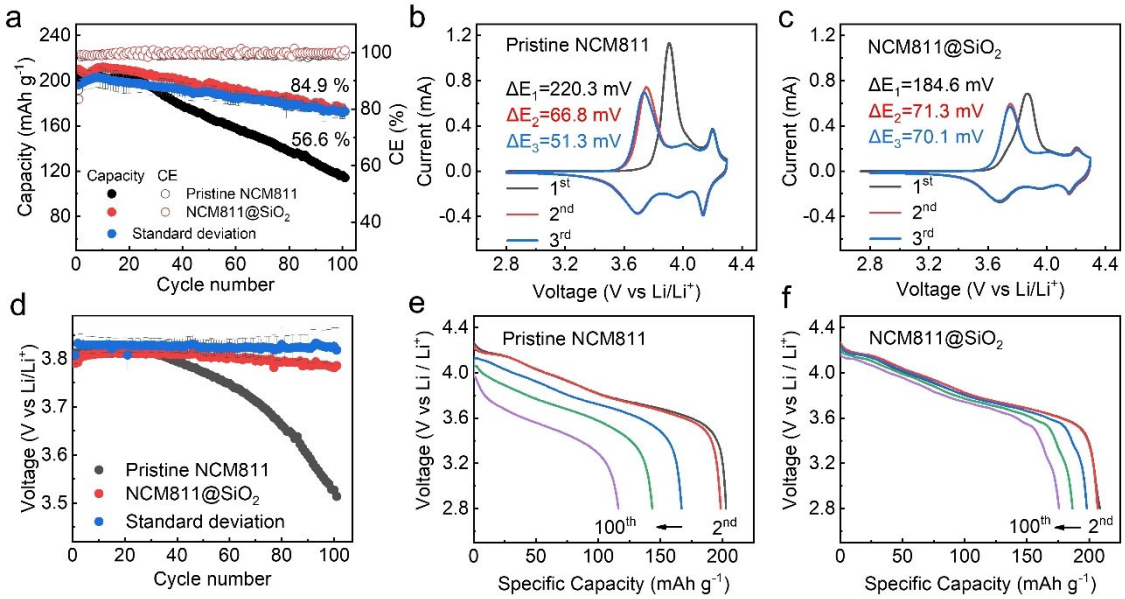

Figure 4. Electrochemical performance of pristine NCM811 and NCM811@SiO_2: cycling stability (a), CV curves for the first three cycles (b, c), discharge midpoint voltage (d) and discharge curves at different cycles (2nd, 25th, 50th, 75th and 100th) (e, f).

electrodes. As shown in Figure 4b, c, both samples display three pairs of redox peaks, corresponding to multiple-phase transformations from the initial hexagonal phase (H1) to a monoclinic structure (M) and two other hexagonal structures (H2 and H3). Minimal deviations in the potential (ΔE) of each anodic and cathodic redox peak suggests minute polarization, indicating highly reversible electrochemical processes for both electrodes.[25] However, for NCM811@SiO_2, the value of ΔE (184.6 mV, 0.1 mV s^{-1}) is lower than that for pristine NCM811 (220.3 mV, 0.1 mV s^{-1}), which indicates that the SiO_2 coating improves the reversibility and kinetics of electrochemical cycling.

A voltage decay during cycling is commonly observed for Ni-rich cathode. The main reason for voltage decay can be attributed into structural deterioration during the cycles. As can be seen in the Figure 4d–f, the discharge voltage and the capacity of the pristine NCM811 decreases rapidly with cycling (Figure 4e). The midpoint voltage during the initial cycle is noted to be 3.81 V but is decreases rapidly to just 3.51 V after 100 cycles. On the contrary, the NCM811@SiO_2 exhibits almost no voltage decay in the same conditions (Figure 4f). It merely decreases from 3.79 to 3.78 V with a 99.7% retention after 100 cycles (Figure 4d). The stable voltage value during cycling further demonstrates that the structural deterioration of NCM811 cathode is effectively suppressed by the SiO_2 surface modification.

The rate capability of pristine NCM811 and NCM811@SiO_2 are compared under various C-rates (0.2–5 C). As illustrated in Figure 5a, the discharge capacity of NCM811@SiO_2 decreased slightly with an increasing rate from 0.2 C to 5 C. A high capacity of 142.7 mA h g^{-1} at a rate of 5 C was obtained, corresponding to a 91.3% of the capacity at 1 C ((Figure 5c). Compared to the rate capability of NCM811@SiO_2, pristine NCM811 exhibits a much lower discharge capacity at the same charging/discharging rate (Figure 5b). A low discharge capacity of 127.9 mA h g^{-1} can be observed at 5 C for NCM811, demonstrating that the SiO_2 greatly influences the cycling stability and rate capability of the NCM811. The enhanced rate capability might be attributed to the stable interface properties that endows the electrode with smaller interfacial impedance.

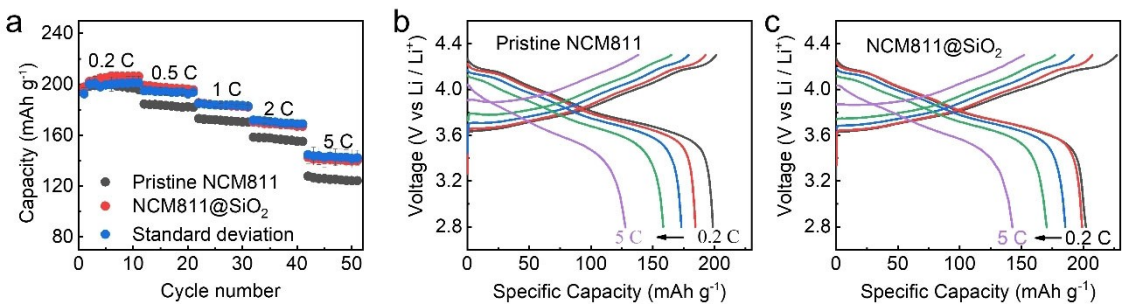

Figure 5. Rate performance (a), the charge-discharge curves of pristine NCM811 (b) and NCM811@SiO_2 (c) at different rate (0.2 C, 0.5 C, 1 C, 2 C and 5 C).

Nyquist plots of electrode impedance spectra (EIS) with different cycles are shown in Figure S5. The high-frequency depressed semicircle presents total resistances of contact and charge transfer. The electrode showed a gradual reduction of the total resistance for the cycled electrode. The charge transfer impedance (R_{ct}) of NCM811@SiO_2 is much lower than that of the pristine NCM811 after 100 cycles.

To advance the understanding of the electrode stability, XRD characterization of the pristine NCM811 and NCM811@SiO_2 electrodes before and after 100 cycles are compared (Figure 6a,b). The NCM811@SiO_2 electrode exhibits, diffraction peaks that are well maintained after 100 cycles. The clear splitting of the (006)/(102) peak and the (108)/(110) peak is observed after 100 cycles, which implying that when the NCM811@SiO_2 cathode maintains its layered structure, thereby demonstrating its excellent structural stability. On the contrary, the splitting peaks of (108)/(110) that disappeared after cycling for the uncoated NCM811, suggesting that its layered structure collapsed during charge/discharge.

In addition to phase changes and chemical attack from the electrolyte that the active particles experience, their damage is another main contributing factor in the deteriorating performance of Ni-rich cathode materials. Figure 6 c-f depicts the SEM images of the pristine NCM811 and NCM811@SiO_2 electrodes after 100 cycles. It is seen that the pristine NCM811 samples undergo considerable pulverization such as pore formation and small cracks (Figure 6c, d). This results from the fact that the delithiation-lithiation induced lattice variations, are accompanied by volume changes and mechanical strains, and therefore damage is commonly observed in NCM811 particles. In contrast

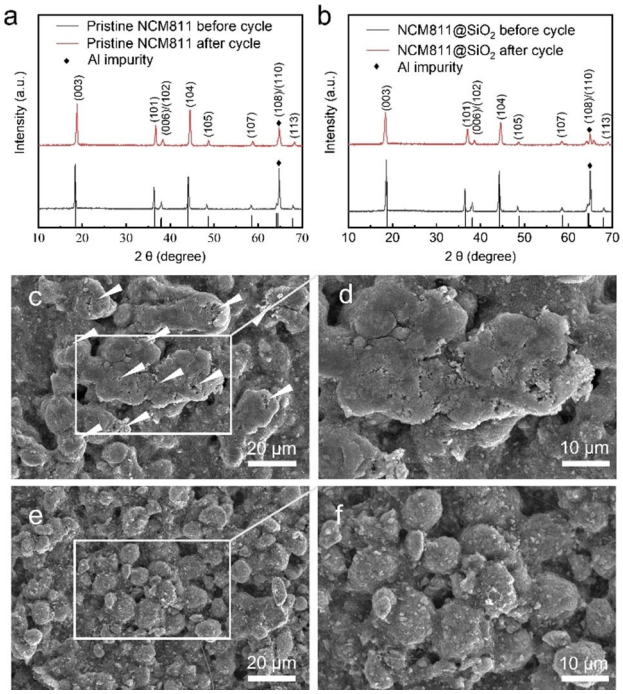

Figure 6. XRD pattern before and after 100 cycles of pristine NCM811 (a) and NCM811@SiO_2 (b). SEM images after 100 cycles of pristine NCM811 (c, d) and NCM811@SiO_2 (e, f).

the NCM811@SiO_2 electrode maintains a good microstructural integrity and no visible morphological changes are seen after 100 cycles (Figure 6e, f).

This is most likely due to the ability of the SiO_2 coating to constrain the volume changes. The occurrence of cracking also results in a larger contact area between the NCM811 particles and electrolyte resulting in the continuous electrolyte decomposition and side reactions, leading to an increase of the impedance and thus poor cycling performance. Furthermore, EDS results (Figure S6) illustrate that the overall content of F and P elements for NCM811@SiO_2 is much lower than that of the pristine NCM811. As the F and P elements mainly comes from the decomposition of $LiPF_6$ contained in the electrolyte, the relatively low content of F and P elements indicates that SiO_2 coating mitigates the decomposition of the constituents of the electrolyte, mainly $LiPF_6$.[26] In addition, the cross-section images of the pristine NCM811 and NCM811@SiO_2 electrodes after 100 cycles are shown in Figure S7. Significant damage is observed in NCM811, while NCM811@SiO_2 retains its morphological integrity.

3. Conclusion

We successfully fabricated uniformly SiO_2 coated NCM811 particles by a urea-assisted homogeneous precipitation method. The electrochemical cycling stability and rate capability of NCM811@SiO_2 are remarkably improved in comparison with the uncoated NCM811 materials. NCM811@SiO_2 exhibits a high-capacity retention of 84.9% after 100 cycles at 0.2 C and excellent rate capability with a capacity of 142.7 mA h g^{-1} at 5 C. This is much higher than that of the pristine NCM811, which has a retention of 56.6% after 100 cycles at 0.2 C, and a discharge capacity of 127.9 mA h g^{-1} at 5 C. The superior electrochemical properties of the proposed NCM811 cathode can be attributed to the uniform and continuous SiO_2 coating that serves as a physical barrier, effectively suppressing the side reactions between electrode and electrolyte. Furthermore, it was shown that SiO_2 coatings can also prevent the fracture and pulverization of the NCM811 secondary particles, which had not been illustrated before. It was, therefore, shown that SiO_2 coatings produced via urea-assisted homogeneous precipitation method is an effective method to enhance the performance of Ni-rich cathode materials for lithium-ion batteries.

Experimental Section

Materials synthesis

$LiNi_{0.8}Co_{0.1}Mn_{0.1}O_2$(NCM811) cathode materials was purchased from Shanshan Corporation., Hunan, China. In preparing the SiO_2 coating, tetraethyl orthosilicate (TEOS, > 99% (GC), Aladdin) was used as the Si source. First a mixed solution of 30 ml ethanol (AR Grade, FTSCI) and deionized water in the volume ratio of 1:1 was prepared and then a stoichiometric amount of TEOS (1 wt.%) was dispersed in it. Dilute nitric acid (HNO_3) was used to adjust the pH value to 1–2, and once the TEOS completely hydrolyzed, ammonium carbonate

solution ($(NH_4)_2CO_3$) was added to adjust the pH of the solution to 6.[20] Subsequently, 2 g NCM811 and 2.4 g urea (AR Grade, SCR) were add to the mixed solution, which was then magnetically stirred at 90 °C for 2 h, followed by filtration, and then washed with deionized water and dried at 80 °C. Finally, the obtained coated NCM811 particles were further heat treated at 500 °C for 5 h in air. The as-prepared modified cathode material was denoted as NCM811@SiO_2.

Material characterization

Powder X-ray diffraction (XRD Smartlab) was used to characterize the crystal structure of all samples with Cu–Kα radiation (λ = 1.5418 Å) in the 2 θ ranging from 10° to 70° with the speed of 4° per minute. Scanning electron microscopy (SEM, SU-3500) equipped with Energy dispersive x-ray spectroscopy (EDS) was used for microstructural analysis. Atomic resolution scanning transmission electron microscopy imaging was performed on an aberration-corrected JEOL-ARM200CF microscope with cold field-emission gun operating at 200 KV. The convergent semi-angle was about 23 mrad and the corresponding collection semi-angle for HAADF-STEM and ABF-STEM images was 90–370 mrad and 11–22 mrad, respectively. Conventional high resolution TEM images were taken by a JEOL F200 microscope with a cold field-emission gun operating at 200 KV. X-ray photoelectron spectroscopy (XPS) was performed to investigate the elemental chemical states of the materials. The Fourier Transform Infrared Spectrometer (FT-IR) spectra of the materials was obtained on a Nicolet 6700 FT-IR Spectrometer (America), using KBr pellets.

Electrochemical measurements

Electrochemical properties were evaluated by utilizing CR2032 type coin cells. Cathodes were fabricated by mixing NCM811@SiO_2 active materials (80 wt.%), super P carbon (10 wt.%), and polyvinylidene fluoride binder (PVDF, ARKEMA) (10 wt.%) in N-methyl-2-pyrrolidone (NMP, Electronic Grade, 99.9%, Aladdin). Enough NMP was added to form the slurry. The electrode was fabricated by coating the slurry on an aluminum foil followed by drying at 120 °C for 8 h in a vacuum oven and then the electrode discs were cut. Lithium metal foil was used as the counter electrode. $LiPF_6$ (1 M) in a 1 : 1 : 1 (v/v/v) ethylene carbonate (EC)/diethyl carbonate (DEC)/ethyl methyl carbonate (EMC) was used as the electrolyte. The cells were assembled in an Ar-filled glovebox. The cells were cycled using a Land instrument battery test system (Wuhan, China) within the potential range of 2.8 and 4.3 V at different current densities. The cyclic voltammetry (CV) measurements were recorded ranging from 2.8 to 4.3 V (vs Li/Li^+) at a various scan rates (0.1 ~ 0.5 mV s^{-1}). Besides, the electrochemical impedance spectroscopy (EIS) of the cell was performed at frequencies between 0.01 Hz and 100 kHz. Both CV and EIS measurements were recorded in the electrochemical workstation (CS2350H, Wuhan CorrTest Instruments Corp., Ltd.). All the tests and measurements were conducted at room temperature.

Acknowledgements

The authors are grateful to the National Natural Science Foundation of China (52002293) and Graduated Innovative Fund of Wuhan Institute of Technology (CX2020157) for supporting this work. KEA, UA are grateful to the National Science Foundation for supporting this work through the CMMI grant (CMMI-1762602).

Conflict of Interest

The authors declare no conflict of interest.

Keywords: cathode materials · coating · Homogeneous precipitation · $LiNi_{0.8}Co_{0.1}Mn_{0.1}O_2$ · Lithium-ion battery

[1] a) C.-H. Jung, D.-H. Kim, D. Eum, K.-H. Kim, J. Choi, J. Lee, H.-H. Kim, K. Kang, S.-H. Hong, *Adv. Funct. Mater.* **2021**, *31*, 2010095; b) T. Kim, W. Song, D.-Y. Son, L. K. Ono, Y. Qi, *J. Mater. Chem. A* **2019**, *7*, 2942–2964; c) M. Li, J. Lu, Z. Chen, K. Amine, *Adv. Mater.* **2018**, *30*, 1800561; d) Z. P. Cano, D. Banham, S. Ye, A. Hintennach, J. Lu, M. Fowler, Z. Chen, *Nat. Energy* **2018**, *3*, 279–289; e) N. Nitta, F. Wu, J. T. Lee, G. Yushin, *Mater. Today* **2015**, *18*, 252–264.
[2] a) H. H. Ryu, N. Y. Park, D. R. Yoon, U. H. Kim, C. S. Yoon, Y. K. Sun, *Adv. Energy Mater.* **2020**, *10*, 2000495; b) J. Kim, H. Lee, H. Cha, M. Yoon, M. Park, J. Cho, *Adv. Energy Mater.* **2018**, *8*, 1702028; c) J. U. Choi, N. Voronina, Y. K. Sun, S. T. Myung, *Adv. Energy Mater.* **2020**, *10*, 2002027; d) B. Wang, F.-I. Zhang, X.-A. Zhou, P. Wang, J. Wang, H. Ding, H. Dong, W.-B. Liang, N.-S. Zhang, S.-Y. Li, *J. Mater. Chem. A* **2021**, *9*, 13540–13551; e) P. Hu, J. Zhao, T. Wang, C. Shang, J. Zhang, B. Qin, Z. Liu, J. Xiong, G. Cui, *Electrochem. Commun.* **2015**, *61*, 32–35.
[3] a) Z. Lun, B. Ouyang, D. H. Kwon, Y. Ha, E. E. Foley, T. Y. Huang, Z. Cai, H. Kim, M. Balasubramanian, Y. Sun, J. Huang, Y. Tian, H. Kim, B. D. McCloskey, W. Yang, R. J. Clement, H. Ji, G. Ceder, *Nat. Mater.* **2020**, *20*, 214–221; b) S. S. Zhang, *J. Energy Chem.* **2020**, *41*, 135–141.
[4] a) H.-H. Ryu, B. Namkoong, J.-H. Kim, I. Belharouak, C. S. Yoon, Y.-K. Sun, *ACS Energy Lett.* **2021**, *6*, 2726–2734; b) C. Xu, P. J. Reeves, Q. Jacquet, C. P. Grey, *Adv. Energy Mater.* **2020**, *11*, 2003404; c) S. Li, X. Fu, Y. Liang, S. Wang, X. A. Zhou, H. Dong, K. Tuo, C. Gao, X. Cui, *ACS Sustainable Chem. Eng.* **2020**, *8*, 9311–9324.
[5] a) J. Kim, H. Cha, H. Lee, P. Oh, J. Cho, *Batteries & Supercaps* **2020**, *3*, 309–322; Supercaps **2020**, 3, 309–322; b) K. Shizuka, C. Kiyohara, K. Shima, Y. Takeda, *J. Power Sources* **2007**, *166*, 233–238.
[6] a) Y.-G. Zou, F. Meng, D. Xiao, H. Sheng, W.-P. Chen, X.-H. Meng, Y.-H. Du, L. Gu, J.-L. Shi, Y.-G. Guo, *Nano Energy* **2021**, *87*, 106172; b) X. Li, L. Jin, D. Song, H. Zhang, X. Shi, Z. Wang, L. Zhang, L. Zhu, *J. Energy Chem.* **2020**, *40*, 39–45.
[7] S.-H. Lee, G.-J. Park, S.-J. Sim, B.-S. Jin, H.-S. Kim, *J. Alloys Compd.* **2019**, *791*, 193–199.
[8] a) S. Hildebrand, C. Vollmer, M. Winter, F. M. Schappacher, *J. Electrochem. Soc.* **2017**, *164*, A2190–A2198; b) P. Mohan, G. P. Kalaignan, *J. Nanosci. Nanotechnol.* **2013**, *13*, 2765–2770; c) Y. Zhao, Z. Lv, T. Xu, J. Li, *J. Alloys Compd.* **2017**, *715*, 105–111.
[9] F. Schipper, H. Bouzaglo, M. Dixit, E. M. Erickson, T. Weigel, M. Talianker, J. Grinblat, L. Burstein, M. Schmidt, J. Lampert, C. Erk, B. Markovsky, D. T. Major, D. Aurbach, *Adv. Energy Mater.* **2018**, *8*, 1701682.
[10] Y. Chen, Y. Zhang, B. Chen, Z. Wang, C. Lu, *J. Power Sources* **2014**, *256*, 20–27.
[11] K. Du, H. Xie, G. Hu, Z. Peng, Y. Cao, F. Yu, *ACS Appl. Mater. Interfaces* **2016**, *8*, 17713–17720.
[12] Y. Fan, J. Wang, Z. Tang, W. He, J. Zhang, *Electrochim. Acta* **2007**, *52*, 3870–3875.
[13] Y.-D. Li, S.-X. Zhao, C.-W. Nan, B.-H. Li, *J. Alloys Compd.* **2011**, *509*, 957–960.
[14] U. Nisar, S. A. J. A. Al-Hail, R. K. Petla, R. A. Shakoor, R. Essehli, R. Kahraman, S. Y. AlQaradawi, D. K. Kim, I. Belharouak, M. R. Amin, *ACS Appl. Energ. Mater.* **2019**, *2*, 7263–7271.
[15] W. Cho, S.-M. Kim, J. H. Song, T. Yim, S.-G. Woo, K.-W. Lee, J.-S. Kim, Y.-J. Kim, *J. Power Sources* **2015**, *282*, 45–50.
[16] G. Zha, Y. Luo, N. Hu, C. Ouyang, H. Hou, *ACS Appl. Mater. Interfaces* **2020**, *12*, 36046–36053.
[17] Q. Gan, N. Qin, Y. Zhu, Z. Huang, F. Zhang, S. Gu, J. Xie, K. Zhang, L. Lu, Z. Lu, *ACS Appl. Mater. Interfaces* **2019**, *11*, 12594–12604.
[18] a) J. Sharma, D. A. Cullen, G. Polizos, K. Nawaz, H. Wang, N. Muralidharan, D. B. Smith, *RSC Adv.* **2020**, *10*, 22331–22334; b) U. Nisar, N. Muralidharan, R. Essehli, R. Amin, I. Belharouak, *Energy Storage Mater.* **2021**, *38*, 309–328.
[19] a) N. Wu, H. Wu, H. Liu, Y. Zhang, *J. Alloys Compd.* **2016**, *665*, 48–56; b) B. Mukherjee, N. Ravishankar, *Nanotechnology* **2007**, *18*, 025603; c) M.

Dirican, M. Yanilmaz, K. Fu, Y. Lu, H. Kizil, X. Zhang, *J. Power Sources* **2014**, *264*, 240–247.
[20] P. P. Ghimire, M. Jaroniec, *J. Colloid Interface Sci.* **2021**, *584*, 838–865.
[21] M. A. Bourebrab, D. T. Oben, G. G. Durand, P. G. Taylor, J. I. Bruce, A. R. Bassindale, A. Taylor, *J. Sol-Gel Sci. Technol.* **2018**, *88*, 430–441.
[22] V. M. Masalov, N. S. Sukhinina, G. A. Emel'chenko, *Inorg. Mater.* **2018**, *54*, 156–162.
[23] Y. Liu, L.-B. Tang, H.-X. Wei, X.-H. Zhang, Z.-J. He, Y.-J. Li, J.-C. Zheng, *Nano Energy* **2019**, *65*, 104043.
[24] I. Saadoune, C. Delmas, *J. Mater. Chem.* **1996**, *6*, 193–199.
[25] S. Guo, B. Yuan, H. Zhao, D. Hua, Y. Shen, C. Sun, T. Chen, W. Sun, J. Wu, B. Zheng, W. Zhang, S. Li, F. Huo, *Nano Energy* **2019**, *58*, 673–679.
[26] Q. Li, Y. Wang, X. Wang, X. Sun, J. N. Zhang, X. Yu, H. Li, *ACS Appl. Mater. Interfaces* **2020**, *12*, 2319–2326.

Manuscript received: September 11, 2021
Revised manuscript received: October 25, 2021
Accepted manuscript online: October 25, 2021